



# Expression and purification of affinity-tagged variants of the photochemical reaction center from *Heliobacterium modesticaldum*

Gregory S. Orf<sup>1,2</sup> · Kevin E. Redding<sup>1,2</sup>

Received: 22 July 2019 / Accepted: 5 September 2019 / Published online: 21 September 2019  
© Springer Nature B.V. 2019

## Abstract

The heliobacterial photochemical reaction center (HbRC) from the chlorophototrophic Firmicutes bacterium *Heliobacterium modesticaldum* is the only homodimeric type I RC whose structure is known. Using genetic techniques recently established in our lab, we have developed a rapid heterologous expression system for the HbRC core polypeptide PshA. Our system relies on rescue of the non-chlorophototrophic  $\Delta pshA::cbp2p-aph3$  strain of *Hbt. modesticaldum* by expression of a heterologous *pshA* gene from a replicating shuttle vector. In addition, we constructed two tagged variants of PshA, one with an N-terminal octahistidine tag and one with an internal hexahistidine tag, which facilitate rapid purification of pure, active HbRC cores in milligram quantities. We constructed a suite of shuttle vectors bearing untagged or tagged versions of *pshA* driven by various promoters. Surprisingly, we found that the *eno* and *gapDH\_2* promoters from *Clostridium thermocellum* drive better expression of *pshA* than fragments of DNA derived from the region upstream of the *pshA* locus on the *Hbt. modesticaldum* genome. This “*pshA* rescue” strategy also provided a useful window into how *Hbt. modesticaldum* regulates pigment synthesis and growth rate when chlorophototrophic output decreases.

**Keywords** Reaction center · Heliobacteria · Epitope-tagging · Membrane protein · Mutagenesis

## Introduction

The protein complex unique to, and required for, chlorophototrophy is the photochemical reaction center (RC), which catalyzes endergonic electron transfer (ET) across a biological membrane using light energy (Blankenship 2014). Chlorophototrophy can be oxygenic (oxygen-producing, using water as a sacrificial electron donor to eventually drive carbon fixation) or anoxygenic (using other electron donors or cyclic electron transfer). However, the anoxygenic type is the evolutionary predecessor to the oxygenic type. Anoxygenic

chlorophototrophy is today maintained by members of six prokaryotic phyla: Acidobacteria, Chlorobi, Chloroflexi, Firmicutes, Gemmatimonadetes, and Proteobacteria. While none of these extant phyla are believed to be the original, anaerobic progenitors of chlorophototrophy (Fischer et al. 2016; Orf et al. 2018), study of the wide diversity of available RCs is important for understanding their complex evolutionary history.

The heliobacteria are the only known family within the phylum Firmicutes capable of chlorophototrophy (Bryant and Frigaard 2006). As members of this phylum, they possess unique genetic and physiological characteristics that distinguish them from the other prokaryotes listed above (Heinzel and Golbeck 2007). The presence of chlorophototrophy in the heliobacteria is most likely the result of an ancient horizontal gene transfer event conferring a gene cluster responsible for chlorophyll and carotenoid biosynthesis and the heliobacterial RC (HbRC) (Sattley et al. 2008; Sattley and Swingley 2013). Therefore, the heliobacteria are a case study in how a minimal chlorophototrophic protein set can fit into an existing anaerobic metabolism to provide a selective benefit. The recent 2.2-Å crystal structure

**Electronic supplementary material** The online version of this article (<https://doi.org/10.1007/s11120-019-00672-3>) contains supplementary material, which is available to authorized users.

✉ Kevin E. Redding  
kevin.redding@asu.edu

<sup>1</sup> School of Molecular Sciences, Arizona State University, Tempe, AZ 85287, USA

<sup>2</sup> Center for Bioenergy and Photosynthesis, Arizona State University, Tempe, AZ 85287, USA

of the HbRC from *Heliobacterium (Hbt.) modesticaldum* answered many outstanding questions about the topology and organization of the HbRC, while posing new questions about the mechanisms of electron transfer and quinone utilization (Gisriel et al. 2017). These new questions should be addressable by the classic structure–function framework utilizing site-directed mutagenesis and biophysical analysis. However, up until the past few years, no protocols for genetic manipulation in any heliobacteria were available.

Recently, our group developed the first tractable genetic engineering system for *Hbt. modesticaldum*. This system allows for transformation with replicating plasmids via conjugation (Baker et al. 2019b), as well as precise gene replacement that leverages the endogenous heliobacterial Type I-A CRISPR-Cas system to autonomously select for the correct transformants (Baker et al. 2019a). We demonstrated chromosomal replacement of the *pshA* gene encoding the HbRC core polypeptide with a gene for kanamycin resistance; the resulting mutant was nonphototrophic and lacked HbRC (Baker et al. 2019a). We reasoned that this  $\Delta pshA::cbp2p\text{-aph3}$  mutant would be a useful platform to express mutant versions of the HbRC without contamination from the wild-type background.

Since isolation of membrane proteins can be a low-yield, time-consuming, and imprecise process, we sought to ease the purification of the HbRC by attachment of a genetically encoded epitope tag that could be selected for via affinity chromatography. The purification process for the HbRC has changed considerably since the early days of study on the heliobacteria. The first attempts were performed on *Helio-bacillus mobilis*, in which HbRC was isolated as a brown band from sucrose density fractionation of detergent-solubilized cell membranes (Trost and Blankenship 1989; van de Meent et al. 1990). This band contained an HbRC complex composed of the PshA core polypeptide dimer and an iron-sulfur di-cluster ferredoxin that would later be named PshB. After the thermophilic *Hbt. modesticaldum* was discovered (Kimble et al. 1995), this species became a model organism for the family and the majority of the work from this point forward focused on its HbRC. Salt-treatment and anion-exchange chromatography were introduced to remove the PshB ferredoxin from the PshA dimer core (Heinnickel et al. 2005) and size-exclusion chromatography was introduced to remove further contaminants (Miyamoto et al. 2006). More recently, the sucrose gradient fractionation step was replaced by tandem anion-exchange and cation-exchange chromatography (Sarrou et al. 2012), which generated HbRC sufficiently homogenous for crystallization and X-ray diffraction, resulting in the 2.2-Å resolution crystal structure (Gisriel et al. 2017). This crystal structure revealed a previously unreported single transmembrane-helix subunit now known as PshX. A review of old SDS-PAGE gels indicates its presence in past preparations, but

its low weight (3.8 kDa) resulted in co-migration on gels with the front band containing pigments, likely precluding its identification (Gisriel et al. 2017). Although the tandem ion-exchange method results in highly purified HbRC, it can strip menaquinone (MQ) molecules from the HbRC, evident by the lack of resolved MQ in the crystal structure (Gisriel et al. 2017; Orf et al. 2018), even though MQ has been found in HbRC preparations in the past (van der Est et al. 1998; Miyamoto et al. 2008; Kondo et al. 2015). Purification methods that maintain MQ occupancy will be required to address the function of the quinones in the HbRC.

Precedents for using deletion/expression systems and affinity chromatography via a polyhistidine tag have been set for RCs, including for the purple bacterial RC (PbRC) (Goldsmith and Boxer 1996), Photosystem II (PSII) (Sugiura and Inoue 1999), Photosystem I (PSI) (Gulis et al. 2008), and the green sulfur bacterial RC (GsbRC) (Azai et al. 2011). Therefore, it was likely that this methodology could be applied to the HbRC. In this paper, we report heterologous expression of two polyhistidine-tagged variants of *pshA* expressed in a *pshA* deletion background. We show that either of these tagged variants allows rapid purification of the HbRC complex in a single step. With these *pshA* expression and rapid HbRC purification methodologies in place, we now have a system for producing site-directed mutants of the HbRC.

## Materials and methods

### Plasmid construction

DNA sequences were maintained electronically using SnapGene<sup>®</sup> software (from GSL Biotech; available at [www.snapgene.com](http://www.snapgene.com)). Kits for PCR purification and plasmid minipreps were obtained from Qiagen USA (Germantown, MD). Unless otherwise noted, all enzymes used for DNA manipulations were obtained from New England Biolabs (Ipswich, MA) and used according to the manufacturer's protocols. In general, Q5 DNA Polymerase was used to amplify DNA via PCR, DpnI was added to restriction digests of PCR amplicons to degrade template DNA, and Quick CIP DNA phosphatase was added to restriction digests of plasmids to prevent recircularization. Desalted oligonucleotides were purchased from Integrated DNA Technologies (Coralville, IA). During construction, plasmids were introduced into *Escherichia coli* strain TOP10 (ThermoFisher, Waltham, MA) using chemical transformation. Recombinant *E. coli* strains were selected in lysogeny broth (LB) at 37 °C using 30 mg L<sup>-1</sup> chloramphenicol, 50 mg L<sup>-1</sup> kanamycin, or erythromycin (300 mg L<sup>-1</sup> on solid media, 100 mg L<sup>-1</sup> in liquid media). A list of oligonucleotides used in this study can

be found in Supplementary Information, Table S1. The *E. coli*-*Clostridia* shuttle vector pMTL86251 (Baker et al. 2019b) was used as the vector backbone for transformation of *Hbt. modesticaldum*.

The *pshA* gene with 300 bp, 500 bp, and 1000 bp of upstream putative promoter region was amplified using the primer pairs *pshAv2-FWD-HindIII + pshAv2-REV-XbaI*, *pshAv3-FWD-HindIII + pshAv2-REV-XbaI*, and *pshAv4-FWD-HindIII + pshAv2-REV-XbaI*, respectively. These amplicons were inserted into the shuttle vector pMTL86251 via restriction cloning into the HindIII and XbaI sites, producing vectors pGO1718, pGO1816, and pGO1817, respectively.

The *pshA* gene from start-to-stop codon was amplified with the primer pair *pshA-FWD-XhoI + pshA-REV-XbaI*. The *eno* promoter (*enop*) from *Clostridium thermocellum* was amplified from pDGO102 (Olson et al. 2015) using primer pair *eno-FWD-HindIII + eno-REV-XhoI*. Expression vector pGO1826 was constructed by triple ligation of pMTL86251 (cut with HindIII and XbaI) with the *pshA* start-to-stop amplicon (cut with XhoI and XbaI) and *enop* amplicon (cut with HindIII and XbaI). The *gapDH\_2* promoter from *C. thermocellum* (*gapDH2p*) was amplified from pDGO095 (Olson et al. 2015) using the primer pair *gapDH\_2-FWD-HindIII + gapDH\_2-REV-XhoI*. Expression vector pGO1833 was constructed like pGO1826, except that the *gapDH2p* fragment was used in place of the *enop* fragment.

To prepare *pshA* genes encoding affinity tags, the *pshA* gene along with a small upstream region was amplified using the primer pair *pshAv2-FWD-HindIII + pshAv2-REV-XbaI* and inserted into the cloning vector pBAD33 using the HindIII and XbaI sites to produce pGO1701. The pBAD33 backbone was used in this instance, because the pMTL86251 backbone is not easily amplifiable by PCR due to an extremely low-GC region in the pIP404 replication module. The primer pair *pshA-his8-link-FWD + pshA-his8-link-REVv2* was used to apply an N-terminal octahistidine tag with a synthetic linker region using the FastCloning protocol (Li et al. 2011), resulting in vector pGO1718. Similarly, the primer pair *pshA-int-his8-FWD + pshA-int-his8-REV* was used to apply an “internal” octahistidine tag, via the FastCloning protocol, in the region encoding for the loop between transmembrane helices 6 and 7 in the mature HbRC. However, sequencing repeatedly revealed that this reaction produced an internal hexahistidine loop instead; this vector was kept as pGO1739. The *i-his6-pshA* gene from pGO1739 was amplified using the primer set *pshA-FWD-XhoI + pshA-REV-XbaI* and triple-ligated into pMTL86251 along with the *eno* promoter using HindIII, XhoI, and XbaI to produce expression vector pGO1828. Similarly, the *n-his8-pshA* gene from pGO1718 was amplified using the primer set *pshAnhis8-FWD-XhoI + pshA-REV-XbaI* and triple-ligated

into pMTL86251 along with *enop* using HindIII, XhoI, and XbaI to produce expression vector pGO1832.

## Transformation of heliobacteria by conjugation

All expression vectors intended for introduction into *Hbt. modesticaldum* were first transformed into *E. coli* strain S17-1 containing the DNA-methyltransferase helper vector pPB347 (Baker et al. 2019b). Transformants were selected on 30 mg L<sup>-1</sup> chloramphenicol and 300 mg L<sup>-1</sup> erythromycin to maintain both plasmids. Single colonies of donor *E. coli* were inoculated into 2 mL of fresh LB liquid containing 30 mg L<sup>-1</sup> chloramphenicol and 100 mg L<sup>-1</sup> erythromycin and grown overnight at 37 °C with shaking at 300 rpm.

All manipulations involving *Hbt. modesticaldum* strains were performed in an anaerobic glovebox (Coy Laboratory Products, Grass Lake, MI) filled with 75% N<sub>2</sub>/20% CO<sub>2</sub>/5% H<sub>2</sub>, and all media were made anoxically (Baker et al. 2019b). All *Hbt. modesticaldum* strains were grown in a Coy Model 2000 forced air incubator set at 50 °C and retro-fitted with 790 nm LED panels; serum vials containing liquid were crimped shut and agar plates were sealed in clear bags to prevent evaporative water loss. Conjugations between donor *E. coli* and recipient *Hbt. modesticaldum*  $\Delta pshA::cbp2p-aph3$  were performed as described (Baker et al. 2019b) with minor modifications. When the *Hbt. modesticaldum*  $\Delta pshA::cbp2p-aph3$  strain (Baker et al. 2019a) was used as the conjugation recipient, on the night before the conjugation, a starter culture grown overnight with kanamycin was diluted 20-fold into a 25-mL serum vial containing a total of 15 mL of PYE (buffered at pH 6.5) containing double the normal concentration of pyruvate (2xP-PYE) and lacking kanamycin, as the conjugation efficiency of this strain drops precipitously when it is maintained under kanamycin selection right up to the time of conjugation (data not shown). After conjugation, dilutions of the cell mixtures were spread on Petri plates containing 2xP-PYE medium (unbuffered), 1.5% noble agar, 10 mg L<sup>-1</sup> erythromycin, and 50 mg L<sup>-1</sup> kanamycin, which were incubated at 50 °C to select for *Hbt. modesticaldum* transconjugants. Recombinant *Hbt. modesticaldum* strains were maintained in liquid in PYE (unbuffered) if capable of chlorophototrophy, or 2xP-PYE (buffered at pH 6.5) if incapable of chlorophototrophy. The concentration of antibiotics used for liquid media were identical to those used for solid media. All constructed strains are listed in Table 1.

## HbRC expression assay

Cultures of WT and recombinant *Hbt. modesticaldum* strains were grown to late log-phase (about 40 h). Aliquots were placed in screw-top 10-mm square glass cuvettes and diluted with fresh media to an OD<sub>788</sub> of ~0.5. Absorbance

**Table 1** *Heliobacterium modesticaldum* strains used in this study

Strain	Genotype and description	Source or reference
<i>Ice1</i> , ATCC 51547	The type strain, isolated from volcanic soil in Iceland	Kimble et al. (1995)
$\Delta pshA::cbp2p-aph3$	$\Delta pshA::cbp2p-aph3$ (Km <sup>r</sup> ); a strain with the entire protein-coding sequence of <i>pshA</i> replaced by the <i>aph3</i> gene driven by the constitutive <i>cbp_2</i> promoter of <i>Clostridium thermocellum</i>	Baker et al. (2019a)
$\Delta pshA::cbp2p-aph3$ [pMTL86251]	$\Delta pshA::cbp2p-aph3$ (Km <sup>r</sup> /Em <sup>r</sup> ); $\Delta pshA::cbp2p-aph3$ bearing the empty shuttle vector pMTL86251	This study
$\Delta pshA::cbp2p-aph3$ [pGO1718]	$\Delta pshA::cbp2p-aph3$ (Km <sup>r</sup> ) <i>pshAp(300 bp)-pshA</i> (Em <sup>r</sup> ); $\Delta pshA::cbp2p-aph3$ bearing plasmid-borne <i>pshA</i> driven by a 300-bp fragment of the chromosome immediately upstream of the native <i>pshA</i> gene	This study
$\Delta pshA::cbp2p-aph3$ [pGO1816]	$\Delta pshA::cbp2p-aph3$ (Km <sup>r</sup> ) <i>pshAp(500 bp)-pshA</i> (Em <sup>r</sup> ); $\Delta pshA::cbp2p-aph3$ bearing plasmid-borne <i>pshA</i> driven by a 500-bp fragment of the chromosome immediately upstream of the native <i>pshA</i> gene	This study
$\Delta pshA::cbp2p-aph3$ [pGO1817]	$\Delta pshA::cbp2p-aph3$ (Km <sup>r</sup> ) <i>pshAp(1000 bp)-pshA</i> (Em <sup>r</sup> ); $\Delta pshA::cbp2p-aph3$ bearing plasmid-borne <i>pshA</i> driven by a 1000-bp fragment of the chromosome immediately upstream of the native <i>pshA</i> gene	This study
$\Delta pshA::cbp2p-aph3$ [pGO1826]	$\Delta pshA::cbp2p-aph3$ (Km <sup>r</sup> ) <i>enop-pshA</i> (Em <sup>r</sup> ); $\Delta pshA::cbp2p-aph3$ bearing plasmid-borne <i>pshA</i> driven by the <i>eno</i> promoter of <i>C. thermocellum</i>	This study
$\Delta pshA::cbp2p-aph3$ [pGO1828]	$\Delta pshA::cbp2p-aph3$ (Km <sup>r</sup> ) <i>enop-ih6-pshA</i> (Em <sup>r</sup> ); $\Delta pshA::cbp2p-aph3$ bearing plasmid-borne <i>pshA</i> with internal hexahistidine tag driven by the <i>eno</i> promoter	This study
$\Delta pshA::cbp2p-aph3$ [pGO1832]	$\Delta pshA::cbp2p-aph3$ (Km <sup>r</sup> ) <i>enop-nh8-pshA</i> (Em <sup>r</sup> ); $\Delta pshA::cbp2p-aph3$ bearing plasmid-borne <i>pshA</i> with N-terminal octahistidine tag driven by the <i>eno</i> promoter	This study
$\Delta pshA::cbp2p-aph3$ [pGO1833]	$\Delta pshA::cbp2p-aph3$ (Km <sup>r</sup> ) <i>gapDH2p-pshA</i> (Em <sup>r</sup> ); $\Delta pshA::cbp2p-aph3$ bearing plasmid-borne <i>pshA</i> driven by the <i>gapDH_2</i> promoter of <i>C. thermocellum</i>	This study

spectra were collected in the 350–1000 nm range. Laser flash-induced P<sub>800</sub> photobleaching transients were collected using a JTS-10 LED kinetic spectrometer (Bio-Logic Inc., Claix, France) equipped with a Continuum Minilite frequency-doubled Nd/YAG laser, as described previously (Sheehy et al. 2018). Using the known extinction coefficient for BChl *g* in the HbRC (van de Meent et al. 1991) and the number of BChl *g* per HbRC (Gisriel et al. 2017), the concentration of HbRC in each culture was calculated using the Beer-Lambert law. This concentration was divided by cell scattering (OD<sub>1000</sub>) to normalize the amount of HbRC to the density of cells. In the course of these experiments, cell densities were always below OD<sub>1000</sub> = 0.5 in order to acceptably normalize the HbRC concentrations. Two biological replicates with three technical replicates each were performed and appropriately averaged for every strain.

### Purification of wild-type HbRC

When needed for comparison to the affinity-tagged versions, wild-type HbRC was purified from the wild-type strain using the method previously used to produce crystallography-grade protein (Gisriel et al. 2017). Purification yields were about 1–2 mg purified HbRC per 1 L of late log-phase culture.

### Purification of polyhistidine-tagged HbRC

Polyhistidine-tagged HbRC was purified by modification of the method used for the WT version (Gisriel et al. 2017). All steps except centrifugations were performed inside a second anaerobic glovebox (Coy Laboratory Products, Grass Lake, MI) filled with 95% N<sub>2</sub>/5% H<sub>2</sub> gas under minimal dim green light. For centrifugations, all bottles and tubes were tightly sealed with tops containing clean rubber gaskets before removal from the anaerobic glovebox. All buffers were deoxygenated by sparging with N<sub>2</sub> gas for at least 2 h before storage in the anaerobic glovebox. All glassware and plasticware were placed into the glovebox at least 24 h before purification in order to remove any oxygen bound to the surface.

Four liters of late log-phase cell culture (40 h after a 1% inoculation) were harvested and subjected to centrifugation at 5000 × *g* for 10 min at 4 °C. After removal of the supernatant, the cells were pooled and resuspended in 35 mL total of ice-cold 50 mM MOPS, pH 7.0 (MB). After repeating the centrifugation and decanting, the mass of the wet cell pellet was measured. The wet cell pellet was resuspended and homogenized in 2 mL of ice-cold MB per gram of cell mass, and lysozyme solution (10 mg mL<sup>-1</sup> in MB) was added to a final concentration of 0.5 mg mL<sup>-1</sup>. The cell suspension was poured into a glass beaker on ice-cold metallic thermal beads (Lab Armor LLC, Cornelius,

OR) and stirred for 30 min in darkness to degrade the peptidoglycan cell wall.

After the lysozyme treatment, an equal volume of MB + 1 M sodium chloride was gently added to the protoplasts to bring the final concentration of sodium chloride to 0.5 M. The protoplasts were broken with sonication using a Branson 450 analog Sonifier (Branson Ultrasonics, Danbury, CT). The thermal beads were replaced with a fresh batch, and stirring was continued, to keep the solution cold during sonication. Sonication was performed for 12 min on a 15% duty cycle and a power setting of 7. The temperature of the solution was measured twice during sonication; the temperature was not allowed to rise above 15 °C.

The broken protoplasts were subjected to centrifugation at  $16,000\times g$  for 10 min at 4 °C. The resulting brown-green supernatant was decanted from the tubes and further subjected to ultracentrifugation at  $150,000\times g$  for 30 min at 4 °C. The resulting orange-brown supernatant containing soluble and peripheral membrane proteins was discarded, leaving a brown-green membrane pellet.

In order to prevent variations in HbRC accumulation from affecting membrane solubilization, we used the mass of the wet membranes to calculate the solubilization conditions rather than BChl *g* absorbance. The mass of the membrane pellet was measured and 10 mL of 50 mM MOPS (pH 7.0) + 0.5 M sodium chloride (MBS) was added per gram of wet membrane pellet. The membrane pellet was gently resuspended using a clean paintbrush until homogenous. (If not used immediately, the membrane suspension could be sealed and stored overnight at 4 °C or long-term at -80 °C.) The membrane suspension was solubilized by dropwise addition of 10% (*w/v*)  $\beta$ -dodecylmaltoside ( $\beta$ -DDM) to a final concentration of 0.91% (*w/v*), and then stirred gently on cold thermal beads for 1 h. The solubilized membranes were then clarified by ultracentrifugation at  $150,000\times g$  for 30 min at 4 °C.

A gravity column containing 30 mL of packed Protein-dex Chemical-Tolerant Ni-Penta Agarose resin (Marvelgent Biosciences Inc., Canton, MA) was washed with 10 column volumes of deionized water in the anaerobic glovebox, and then equilibrated with 10 column volumes of MBS + 0.02%  $\beta$ -DDM. The clarified, solubilized membrane solution was directly loaded onto the column and allowed to flow over the resin by gravity. The effluent was re-applied to the top of the column and allowed to pass through the resin once more to facilitate complete binding. At this point, a dark green band had formed on the top of the resin and the effluent was yellow-brown.

The column was successively washed with 5 column volumes of MBS + 0.02%  $\beta$ -DDM and 5 column volumes of MBS + 0.02%  $\beta$ -DDM + 10 mM imidazole. Bound protein was eluted with MBS + 0.02%  $\beta$ -DDM + 100 mM imidazole. The eluted protein (~ 30 mL) was concentrated using

100-kDa MWCO Amicon centrifugal filters (Millipore-Sigma, Burlington, MA) down to 2 mL. The protein was passed through a PD-10 desalting column (GE Healthcare, Chicago, IL) pre-equilibrated with MB + 0.02%  $\beta$ -DDM and finally concentrated down to ~0.5 mL using the aforementioned centrifugal filters. Purified HbRC could be stored at room temperature in the dark in the anaerobic glovebox for at least six months without noticeable degradation.

## Polyacrylamide gel electrophoresis

SDS-PAGE was performed using the Tris–Tricine gel system as described previously (Schägger 2006). For each HbRC variant, 5  $\mu$ L of protein solution at  $OD_{787} = 10$  and  $OD_{787} = 1$  (determined to contain 8.5 pmol and 0.85 pmol of protein, respectively (Sarrou et al. 2012)) were solubilized with 5  $\mu$ L Coomassie loading buffer (with added reductant). All 10  $\mu$ L of each sample were loaded onto a gel composed of a 15% polyacrylamide resolving layer and 4% polyacrylamide stacking layer. Voltage was applied to the gel system at 30 V for 30 min, and then 120 V until sufficient separation had occurred. For publication-quality images, the gels were silver-stained and photographed according to a method described previously (Chevallet et al. 2006), except that 12% (*v/v*) glutaraldehyde was used as the fixative instead of formaldehyde.

Peptide fingerprinting of gel bands was performed at the OKED Mass Spectrometry Core Facility at Arizona State University's Biodesign Institute. For these experiments, gels were stained with Coomassie Brilliant Blue (CBB) stain without added fixative (Schägger 2006) instead of silver staining. After excision of the proper gel band with a scalpel, a standard in-gel trypsin digestion protocol was performed (Shevchenko et al. 2006), followed by C-18 zip-tip purification of the resulting tryptic peptides. Peptide analysis was performed on an Orbitrap Fusion Lumos Tribrid mass spectrometer with an Ultimate 3000 Nano-LC and nano-electrospray ionizer (ThermoFisher Scientific, Waltham, MA). The LC experiment used an Acclaim PepMap 100 C-18 analytical column (3  $\mu$ m particle, 100 Å pore, 75  $\mu$ m i.d.  $\times$  150 mm) and a 150-min buffer gradient with a flow rate of 300 nL min<sup>-1</sup>. Data-dependent mass spectra acquisition in positive mode was performed for data collection. The resultant fragmentation ion spectra were searched with Proteome Discoverer 2.2 using the SEQUEST search engine on the UniProt proteome entry for *Hbt. modesticaldum* strain Ice1 (<http://www.uniprot.org>) and the manually-added *ih6-pshA* translated protein sequence. For search parameters, trypsin cleavage with up to two missed cleavage sites were allowed, and precursor and fragment mass tolerances were set at  $\pm 10$  ppm and 0.6 Da, respectively. Carbamidomethyl modification of cysteine was set as a fixed modification and oxidation of methionine was set as a variable modification.

## Steady-state spectroscopy

Steady-state absorbance spectra of heliobacterial cells and purified protein were collected as described previously (Baker et al. 2019a) using a fiber optic spectrometer (StellarNet, Inc., Tampa, FL) equipped inside the anaerobic glovebox. The spectrometer was composed of a SL1 Tungsten source lamp, SL3 Deuterium source lamp, and SR-50 concave holographic grating detector unit. The light outputs from the SL1 and SL3 lamps were joined using a Y-cable to generate a broad spectral range. The lamp light was carried to a CUV1 cuvette holder using the Y-cable and transmitted light was carried to the detector unit by a second fiber optic cable. Fresh PYE media (for cells) or MB + 0.02%  $\beta$ -DDM (for purified protein) were used to blank the spectrometer. A 10-mm square glass cuvette was used for cells and a 10-mm square quartz cuvette was used for purified protein.

## Cofactor analysis by HPLC

To extract the non-covalently bound cofactors of the purified HbRCs, 140  $\mu$ L of deoxygenated 1:1 acetone:methanol was added to 10  $\mu$ L of concentrated HbRC in a microfuge tube. The solution was vortexed thoroughly and subjected to centrifugation at 13,000 $\times$ g for 1 min. To extract pigments from whole cells, 1 mL of actively-growing culture was centrifuged at 13,000 $\times$ g for 1 min in a microfuge tube. Five-hundred microliters of deoxygenated 1:1 acetone:methanol was added and the solution was vortexed thoroughly and subjected to further centrifugation at 13,000 $\times$ g for 1 min. All extracts were filtered through a solvent-resistant 0.2- $\mu$ m filter prior to injection (100  $\mu$ L) into the HPLC system.

The HPLC system consisted of a PhenoSphere C-18 analytical reverse phase column (part number 00G-3172-E0, Phenomenex Co., Torrance, CA) attached to a Jasco HPLC system described previously (Kashey et al. 2018). A diode array detector was set to measure an absorbance spectrum of the column effluent in the 200–900 nm range (in 1 nm increments) once per second. To analyze the quinone content of purified HbRCs, a chromatographic protocol using a 1.5 mL min<sup>-1</sup> isocratic flow of 94:6 methanol:hexanes was used (Kashey et al. 2018). To calculate the concentrations of MQ-8, MQ-9, menaquinol-9 (MQH<sub>2</sub>-9), and 4,4'-diaponeurosporene (4,4'-DANS), chromatograms at 246 nm and 440 nm were extracted and the corresponding peaks integrated using Origin 2015 (OriginLab Corp., Northampton, MA). A unique peak for MQH<sub>2</sub>-8 could not be identified because it overlaps with the (B)Chl peak. The known extinction coefficients for each species (Sarrou et al. 2012) were then used to calculate their concentration in each sample ( $\epsilon_{260}$  (MQ-8/9) = 15 mM<sup>-1</sup> cm<sup>-1</sup>, extrapolated to 21 mM<sup>-1</sup> cm<sup>-1</sup> at 246 nm;  $\epsilon_{246}$  (MQH<sub>2</sub>-9) = 45 mM<sup>-1</sup>

cm<sup>-1</sup>;  $\epsilon_{440}$  (4,4'-DANS) = 150 mM<sup>-1</sup> cm<sup>-1</sup>,  $\epsilon_{754}$  (BChl g) = 89 mM<sup>-1</sup> cm<sup>-1</sup>).

To analyze the whole-cell pigment content, a chromatographic protocol using a dual solvent gradient was used (Siefermann-Harms 1988; Baker et al. 2019a). Briefly, two solvents were prepared: Solvent A was composed of 74:6:1 acetonitrile:methanol:0.2 M Tris-HCl (pH 8.0), and Solvent B was composed of 7:1 methanol:hexane. The flow rate was set at 1.0 mL min<sup>-1</sup> for the entire experiment and the column was equilibrated with Solvent A. After sample injection, the following chromatography protocol was performed: isocratic flow of Solvent A (0–8 min), linear gradient from 100% Solvent A to 100% Solvent B (8–18 min), isocratic flow of Solvent B (18–36 min), and linear gradient from 100% Solvent B to 100% Solvent A (36–40 min).

## Results

### Cloning and transformation strategy

We recently succeeded in establishing a tractable genetic system for *Hbt. modesticaldum*, complete with stably replicating shuttle vectors and chromosomal gene replacement (Baker et al. 2019b). The initial case study was replacement of the *pshA* gene coding for the core polypeptide of the HbRC (Baker et al. 2019a). While the resulting  $\Delta pshA::cbp2p\text{-}aph3$  mutant was of interest for study of the non-phototrophic metabolic pathways in the organism, it is also useful as a platform for a HbRC mutagenesis system. In this study, we developed a “*pshA* replacement strategy”, in which a heterologous copy of *pshA* gene on a replicating shuttle vector is introduced into the  $\Delta pshA::cbp2p\text{-}aph3$  strain, thereby ensuring that the only version of the PshA core polypeptide in the cell is encoded by the plasmid-borne gene. Use of a replicating vector also provides a quick way to test the strength of various promoter elements.

Using the pMTL modular shuttle vector platform (Heap et al. 2009), we constructed pMTL86251 using modules purchased from Chain Biotech Ltd. (Marlow, UK). This particular variant contains a Gram-positive replication origin from the pIP404 plasmid found in *Clostridium perfringens* (Garnier and Cole 1988; Sloan et al. 1992), which is the only Gram-positive replication origin that we have found to be compatible with *Hbt. modesticaldum* (Baker et al. 2019b). Using pMTL86251 as a backbone, we cloned five different promoters upstream of the *pshA* gene. Among these five, three originated from the region directly upstream of the *pshA* gene on the *Hbt. modesticaldum* chromosome. The *pshA* gene is one of the most highly-expressed protein-coding genes in this organism and its transcript levels are much higher than those of the (B)Chl synthesis genes surrounding it (Sheehy et al. 2018), so we reasoned that there must

be a strong promoter in this region. The other two promoters tested, *eno* and *gapDH\_2*, were previously identified as strong promoters in *Clostridium thermocellum*, but relatively weak promoters in *E. coli* (Olson et al. 2015), thus facilitating cloning of genes that are potentially lethal to *E. coli*. Restriction sites (HindIII and XhoI) were cloned into the ends of each promoter to allow for the insertion of the wild-type *pshA* gene downstream (Fig. 1).

### Tag placement strategy

As the N-termini of both PsaA of PSI and PscA of the GsbRC have been modified with polyhistidine tags (Gulis et al. 2008; Azai et al. 2011), we believed that a similar tagging strategy would be successful for the HbRC. Our strategy placed a polyhistidine tag in front of a 15-residue flexible linker region. Since the soluble portion of the native N-terminus of the PshA polypeptide is not as long as its counterpart in PsaA or PscA, and may be close to the main transmembrane structure of the protein, we felt it prudent to include a flexible linker region to increase access of the tag to the affinity resin. Thus, for the N-terminal octahistidine tag, we inserted a total of 27 amino acids directly in front of the natural N-terminal methionine (Fig. 2a). The resulting HbRC with an N-terminal His<sub>8</sub> tag on each PshA polypeptide was termed NH-NH-HbRC.

We also tried a riskier tagging strategy, in which a tag was placed in an internal loop of the protein. A long cytoplasmic loop was identified in the crystal structure between transmembrane helices (TMH) 6 and 7. The first 11 amino acids of this loop are relatively unstructured and exposed to the cytoplasm, so six histidine residues were simply inserted with no additional linkers. This region is not predicted to interact with soluble ferredoxins, so a short insertion was not expected to interfere with electron transfer out of the HbRC (Fig. 2b). The resulting HbRC with an internal His<sub>6</sub> tag on each PshA polypeptide was termed IH-IH-HbRC.

### Promoter screening

Expression vectors pGO1718, pGO1816, pGO1817, pGO1826, and pGO1833 were constructed containing the wild-type *pshA* gene driven by the putative *pshA* promoters (300, 500, and 1000 bp), *eno* promoter, and *gapDH\_2* promoter, respectively. These vectors were transformed into *Hbt. modesticaldum*  $\Delta pshA::cbp2p-aph3$  (Baker et al. 2019b). Upon cursory visual inspection, in some strains the light green color normally seen in the  $\Delta pshA::cbp2p-aph3$  strain became more brown, closer to that of the wild-type, presumably due to the presence of assembled HbRC.

Cultures in late log growth phase were analyzed for their overall HbRC content by quantifying the concentration of

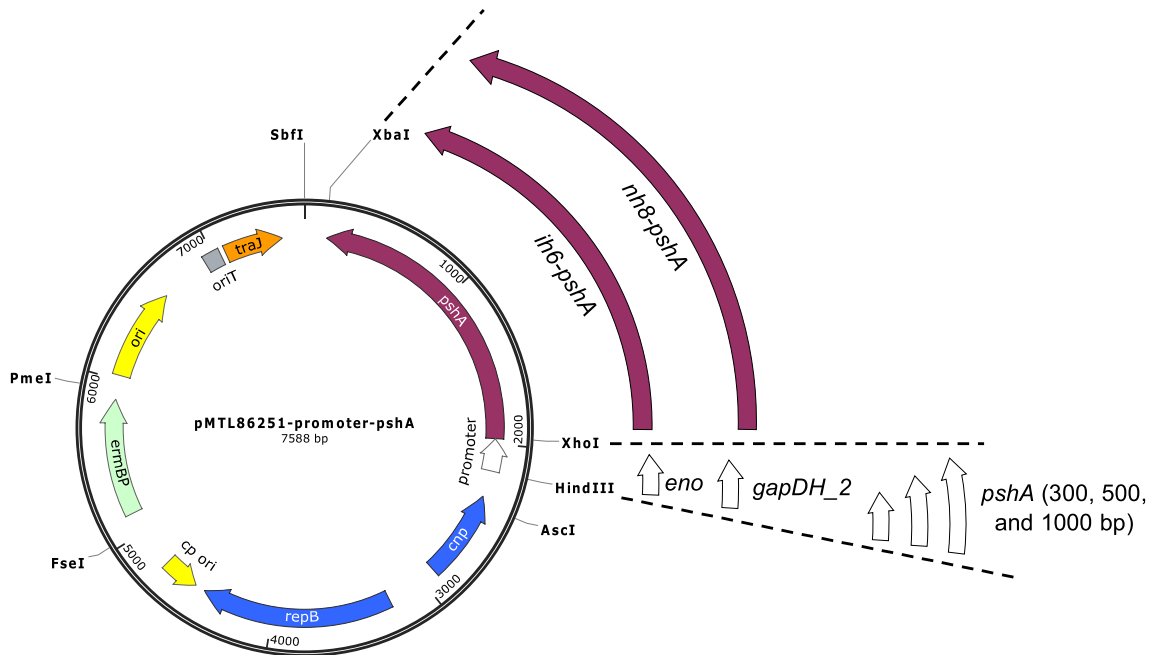
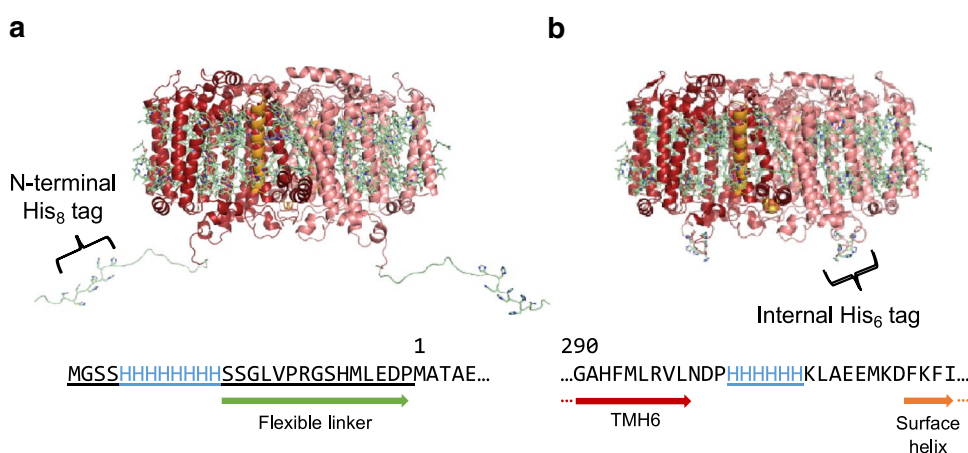


**Fig. 1** Shuttle vector design for expression of heterologous *pshA* genes in *Hbt. modesticaldum*  $\Delta pshA::cbp2p-aph3$ . The plasmid backbone is pMTL86251, which is stably maintained in *Hbt. modesticaldum* (Baker et al. 2019b). *repB*: replication initiation protein from *Clostridium perfringens* plasmid pIP404. *cp ori*: origin of replication from *C. perfringens* plasmid pIP404. *cnp*: copy-number regulator

protein from *C. perfringens* plasmid pIP404. *ermBP*: rRNA adenine N-6-methyltransferase from *C. perfringens* conferring erythromycin resistance. *ori*: ColE1 origin of replication. *oriT*: origin of transfer from plasmid RP4. *traJ*: positive regulator of conjugal transfer from plasmid RP4. Unique restriction sites used for plasmid assembly are indicated

**Fig. 2** Models of the HbRC containing polyhistidine tags in the PshA polypeptides. **a** N-terminal His<sub>8</sub> tag separated from the main structure of the protein by a flexible linker (NH-NH-HbRC). **b** Internal His<sub>6</sub> tag inserted in a flexible cytoplasmic loop between TMH6 and TMH7 (IH-IH-HbRC). Underlined regions are insertions. Models were created via homology to the published HbRC structure (PDB code 5V8 K) using SWISS-MODEL (<https://swissmodel.expasy.org/>)



the P<sub>800</sub> special pair using the JTS-10 kinetic spectrometer. This pump-probe spectroscopic assay provides a sensitive measurement of maximal photobleaching of P<sub>800</sub> after a saturating laser pulse, which can be mathematically related back to the overall concentration of the HbRC in the sample. Further, we normalized the experimentally-derived HbRC concentration back to a standard number of cells as measured by cell scattering at 1000 nm. The results allow for a straightforward comparison of promoter strength and show that this method can be used as a general assay to measure the strength of any promoter in *Hbt. modesticaldum* (Fig. 3).

Cultures of wild-type *Hbt. modesticaldum* at an OD<sub>1000</sub> = 1 contained HbRC at a concentration of 108 ± 2.2 nM. The  $\Delta pshA::cbp2p\text{-}aph3$  strain had no measurable P<sub>800</sub> photobleaching and thus accumulated no functional HbRC (Fig. 3), as expected. The  $\Delta pshA::cbp2p\text{-}aph3$  strain harboring the empty shuttle vector pMTL86251 also exhibited no measurable P<sub>800</sub> photobleaching (Fig. 3). When the  $\Delta pshA::cbp2p\text{-}aph3$  strain was conjugated with pGO1718, pGO1816, and pGO1817 (bearing *pshA* driven by various lengths of the putative endogenous *pshA* promoter), mature HbRC accumulated only to about 1–3% of the level of that in the wild-type strain (Fig. 3). In contrast, using the *C. thermocellum eno* and *gapDH\_2* promoters resulted in much higher expression of *pshA*. The *eno* promoter drove expression of HbRC to a steady-state level of ~30% of the wild-type strain and the *gapDH\_2* promoter was more than twice as effective. Among the strains driving *pshA* expression from the *eno* promoter, the strain bearing the N-terminally octahistidine-tagged variant accumulated a slightly higher steady-state concentration of HbRC.

Growth trials were performed on selected strains from the above experiment to determine how the levels of HbRC expression affected doubling time or cell abundance at stationary phase (Supplementary Information, Fig. S1). These trials showed that the final cell density at stationary phase increases with increasing HbRC levels.

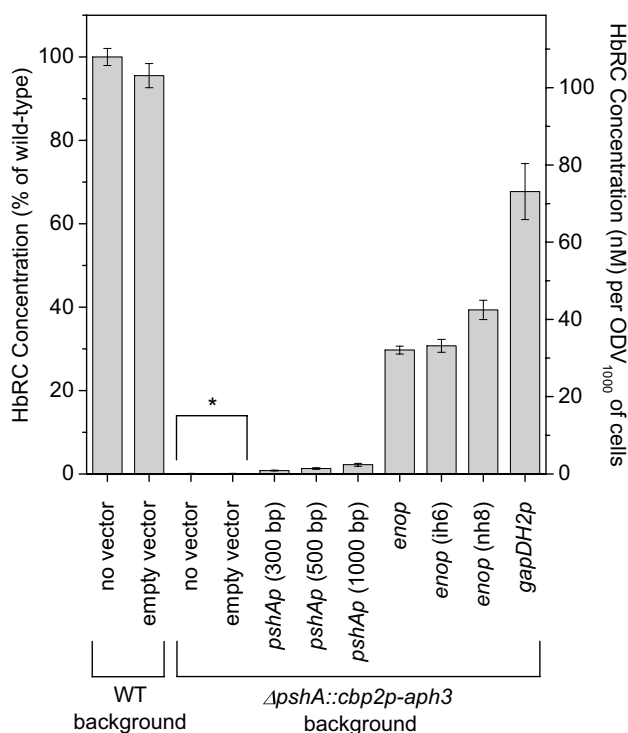


**Fig. 3** Quantification of accumulated HbRC in the various strains used in this study. HbRC concentration in a given cell sample was quantified by P<sub>800</sub> photobleaching with a saturating laser flash, then scaled to the sample's respective OD<sub>1000</sub> to provide a HbRC concentration normalized to cell density. For the *pshA* rescue strains (in the chromosomal  $\Delta pshA::cbp2p\text{-}aph3$  background), the promoter used to drive *pshA* expression is listed, as well as the affinity tag on *pshA*, if included. The asterisk (\*) denotes strains in which a statistically negligible signal was detected

### Purification of polyhistidine-tagged HbRC complexes

The initial steps in purification of polyhistidine-tagged HbRC complexes was carried out similarly to the unmodified HbRC, except that 0.5 M NaCl was added to all buffers



after lysozyme treatment, in order to remove any soluble membrane-associated proteins from the membrane. In the standard method, detergent-solubilized membranes were passed through a DEAE-Sepharose anion-exchange resin, resulting in removal of the PshB-type ferredoxins from the HbRC. This step was thus unnecessary, as salt-washing results in removal of PshB1 from the HbRC (Heinzel et al. 2005). This allowed us to bind affinity-tagged HbRC to the affinity column without interference or significant contamination from the PshB ferredoxins.

Optimization of the imidazole washing steps was performed as well. Both tagged variants of the HbRC began to elute after addition of 30 mM imidazole. Therefore, washing steps were limited to 10 mM imidazole and complete elution was performed using 100 mM imidazole. SDS-PAGE analysis of the polypeptides in the preparations indicated similar purity to unmodified HbRC purified via tandem ion-exchange chromatography (Fig. 4). Both the PshA and PshX polypeptides could be clearly resolved. In the IH-IH-HbRC and NH-NH-HbRC samples, additional weak bands corresponding to ferredoxin (potentially PshB1 and/or PshB2) and cytochrome  $c_{553}$  could be seen when high concentrations of protein were loaded to visualize PshX. Since these bind the HbRC in the membrane, it is unsurprising that a small amount of these proteins is pulled down in the affinity chromatography experiment.

Some additional polypeptides could be seen in the IH-IH-HbRC and NH-NH-HbRC samples. The weak bands directly below the main PshA band in both samples are likely proteolysis products of PshA that co-purify with the intact complex. In the IH-IH-HbRC sample, a strong band is also seen at ~25 kDa. In-gel trypsin digestion and subsequent mass spectrometric analysis was performed on this band, which

confirmed the presence of peptides derived from internally hexahistidine-tagged PshA (Supplementary Information, Fig. S2). Thus, we conclude that this band constitutes proteolysis products as well. Cleavage near the site of the hexahistidine tag would result in production of two polypeptides having roughly the same molecular mass. The intact PshA polypeptide migrates anomalously on SDS-PAGE (~68 kDa calculated mass versus ~50 kDa apparent mass) due to its hydrophobic nature, so it is unsurprising that proteolysis products with a calculated mass of ~34 kDa will migrate with an apparent size of ~25 kDa.

### Photochemical activity and cofactor composition of NH-NH-HbRC and IH-IH-HbRC

In the absorbance spectra of NH-NH-HbRC and IH-IH-HbRC, the major absorbance peaks of BChl  $g$  (370 nm, 577 nm, and 787 nm) and  $8^1$ -OH Chl  $a$  (672 nm) are the same as for unmodified HbRC (Fig. 5a). A consistently small level of additional absorbance is observed in the 250–670 nm range in the affinity-purified variants. A difference spectrum (Fig. 5a, inset) reveals this to be a small contamination of free pheophytin (Pheo)  $a$ . This is unsurprising given that it was previously shown that the cation-exchange chromatography step was required to remove free Pheo  $a$  from the HbRC (Sarrou et al. 2012), a step that was omitted in this preparation.

Millisecond time-resolved transient absorbance spectroscopy was used to monitor the photo-oxidation and recovery of  $P_{800}$  upon a saturating laser flash. In purified HbRC samples, the main mechanisms for  $P_{800}$  photobleaching recovery on the ms-sec timescale are charge recombination (CR) from the  $P_{800}^+F_X^-$  state and re-reduction of  $P_{800}^+$  by an added

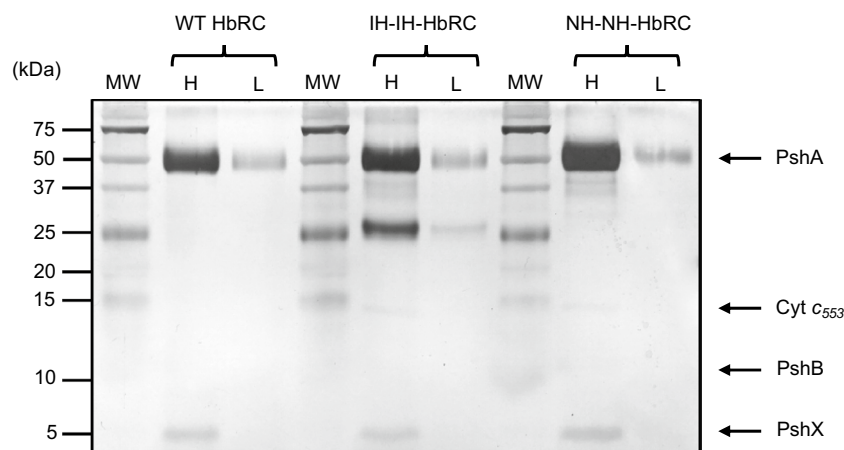
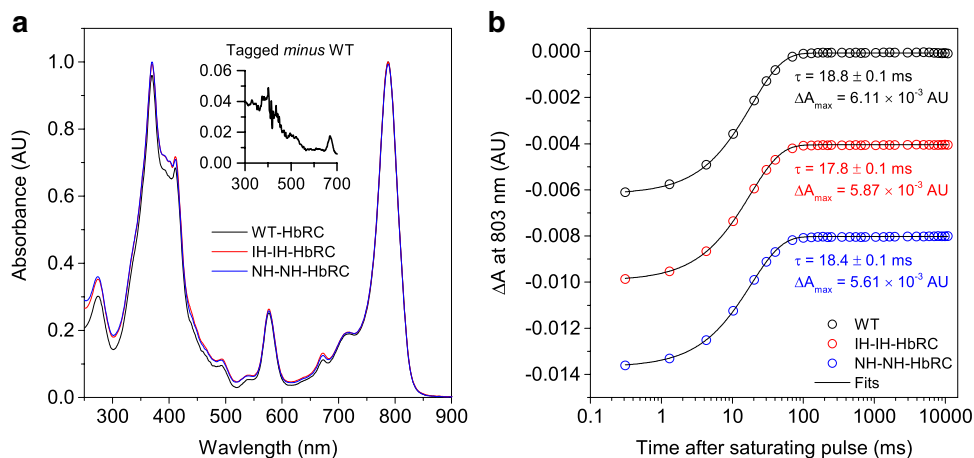


**Fig. 4** SDS-PAGE analysis of purified wild-type and affinity-tagged HbRC. Separation was performed on a 15% polyacrylamide gel and silver staining was performed to visualize bands. Each HbRC variant was loaded in high concentration (H) corresponding to ~450 pmol

BChl  $g$  (~8.5 pmol protein) and low concentration (L) corresponding to ~45 pmol BChl  $g$  (~0.85 pmol protein). Due to its small size, the PshX polypeptide could only be visualized at higher concentration. MW: molecular weight markers (sizes indicated on the left side)

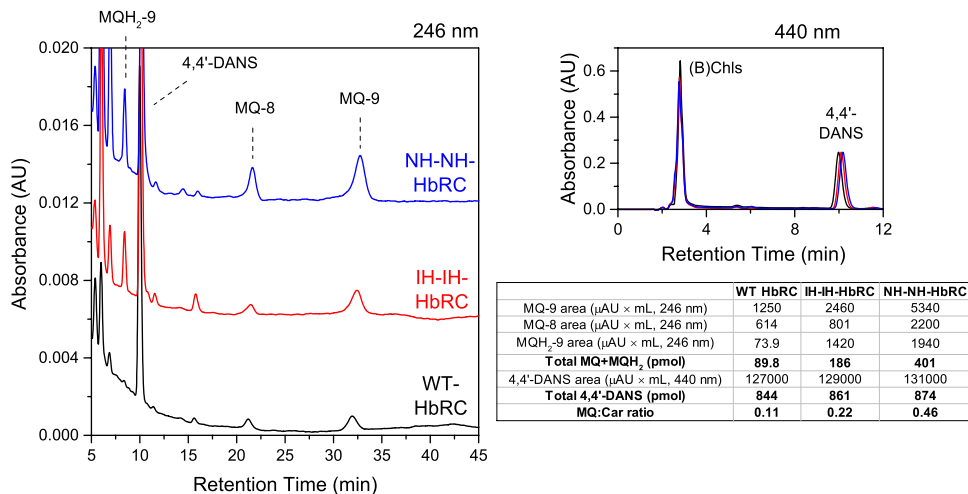
**Fig. 5** Spectroscopic analysis of affinity-tagged HbRC variants. **a** Steady-state absorbance, and **b**  $P_{800}$  photobleaching recovery kinetics in the millisecond-to-second time range as measured by a Joliot-type spectrometer. In **b**, plots are offset by 0.003 AU for clarity. Each sample was adjusted to the same BChl *g* concentration (9.1  $\mu\text{M}$ ) such that  $\text{OD}_{787} = 1.0$



reductant, such as ascorbate. Since reductant was not added to these samples, and the samples were incubated in the dark before the experiment, the main mechanism is expected to be CR. In purified WT HbRC, CR from the  $P_{800}^+F_X^-$  state has been observed to occur with a primary kinetic component ranging from ~12 to 20 ms (Heinnickel et al. 2005, 2007; Sarrou et al. 2012; Redding et al. 2014). Consistent with these findings, we observe CR in the WT HbRC as a single kinetic component with a time constant of  $18.8 \pm 0.1$  ms (Fig. 5b). For IH-IH-HbRC and NH-NH-HbRC purified via affinity chromatography, CR is observed with decay times of  $17.8 \pm 0.1$  ms and  $18.4 \pm 0.1$  ms, respectively (Fig. 5b). These CR rates are consistent with what is expected from functional HbRC cores. Additionally, the ratio of the maximal amount of  $P_{800}$  photobleaching to gross BChl *g* absorbance (at 787 nm) is nearly identical for all three samples ( $\Delta A_{803} \sim 6$  mAU for  $\text{OD}_{787} = 1$ ), indicating that antenna sizes are unchanged by the presence of the tags and that the preparations of tagged HbRC do not contain detectable amounts of inactive protein.

Because both the presence and function of MQ in the HbRC have been debated in the literature, we quantified the amount of MQ-8, MQ-9, and MQH<sub>2</sub>-9 in the purified HbRC variants via HPLC (Fig. 6). We compared samples with equal amounts of the carotenoid, 4,4'-diaponeurosporene (4,4'-DANS), two molecules of which are present in each HbRC (Gisriel et al. 2017). We integrated the area under each peak of interest and calculated a total MQ + MQH<sub>2</sub> concentration and 4,4'-DANS concentration using the known extinction coefficients of each species (see Materials and Methods). Based on this, each 100- $\mu\text{L}$  sample contained between 844 and 874 pmol of 4,4'-DANS. The WT HbRC, IH-IH-HbRC, and NH-NH-HbRC samples contained 89.8 pmol, 186 pmol, and 401 pmol total MQ + MQH<sub>2</sub>, respectively, yielding MQ:Car ratios of 0.11, 0.22, and 0.46. This indicates that the affinity chromatography treatment results in quinone occupancy that is 2-to-4-fold higher than what is observed in the WT HbRC purified by tandem ion-exchange chromatography. Because we could not resolve

**Fig. 6** HPLC analysis of the quinone content of affinity-tagged HbRC variants. Chromatograms measured at 246 nm (offset by 0.06 AU to facilitate comparison) and 440 nm are shown with relevant peaks labeled. The chromatogram at 440 nm confirms loading of samples with nearly equal 4,4'-DANS. Calculations of MQ:Car ratios are shown in the table inset



a peak corresponding to MQH<sub>2</sub>-8, our quinone occupancy calculations are likely on the conservative end.

### The relationship between *pshA* expression level and whole-cell pigment distribution

In the WT strain, the stoichiometry of accumulating pigments (Fig. 7, top chromatogram) in whole cells closely follows the pigment composition of the HbRC: mostly BChl *g* with a small contribution from BChl *g'*, 8<sup>1</sup>-OH Chl *a*, and 4,4'-DANS. In addition, some bacteriopheophytin (BPheo) *g* is seen, as well as some mixed hydrophilic pigments, such as bacteriochlorophyllides (BChlides) and bacteriopheophorbides (BPhs). In the  $\Delta pshA::cbp2p-aph3$  strain (Fig. 7, middle chromatogram), some of these pigments are greatly diminished or absent; the major accumulating pigments were BPheo *g* and 4,4'-DANS with a small (but greater than WT) contribution from 8<sup>1</sup>-OH Pheo *a*, and BChlides/BPhs. BPheo *g*, in particular, is enriched in the  $\Delta pshA::cbp2p-aph3$  strain compared to the WT. When phototrophy in the  $\Delta pshA::cbp2p-aph3$  strain is rescued by conjugation with pGO1826 (Fig. 7, bottom chromatogram), and HbRC levels rise back to ~30% of WT levels, BChl *g/g'* and 8<sup>1</sup>-OH Chl *a* partially return with a corresponding decrease in BPheo *g*, 8<sup>1</sup>-OH Pheo *a* and BChlides/BPhs.

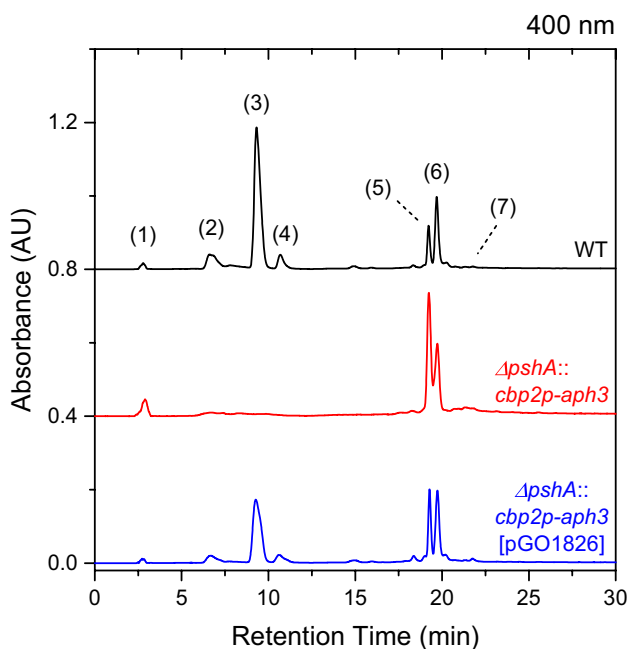


**Fig. 7** HPLC analysis of the whole-cell pigment content of wild-type *Hbt. modesticaldum* and mutants. The peaks were identified as follows: (1) mixed hydrophilic pigment products, such as (B)Chlides and (B)Phs, (2) 8<sup>1</sup>-OH Chl *a*, (3) BChl *g*, (4) BChl *g'*, (5), BPheo *g*, (6) 4,4'-DANS, (7) 8<sup>1</sup>-OH Pheo *a*. The chromatograms are normalized to the peak corresponding to 4,4'-DANS and offset by 0.4 AU to facilitate comparison

## Discussion

The approach outlined in this study allows for rapid purification of HbRC devoid of most contaminants (Fig. 4). Both tagged variants of the HbRC were expressed and accumulated at a similar level as the unmodified HbRC when driven by the Clostridial *eno* promoter (Fig. 3). Additionally, spectroscopic and functional analysis of the affinity-purified protein showed essentially no differences from the untagged version (Fig. 5). Overall, these data indicate that the tagging affected neither the global folding of the PshA polypeptide nor assembly of the homodimer. Retention of menaquinone was increased in the affinity chromatography-prepared HbRCs (Fig. 6), indicating that the gentler purification conditions do not strip the menaquinone as harshly as the ion-exchange steps previously used. We conclude that in the purification method developed for crystallography (Gisriel et al. 2017), the second addition of  $\beta$ -DDM detergent to the sample after the anion-exchange chromatography step (which facilitates binding of the HbRC to the cation-exchange column), is partially responsible for the lowered occupancy of menaquinone. The affinity purification protocol described here neither includes nor requires this step. We are still unsure of the physical location of the menaquinone in our preparations, but it is clear that menaquinone is not found inside the HbRC after crystallization (Gisriel et al. 2017). It is therefore likely that at least some, if not all, of the menaquinone present in HbRC preparation binds to the exterior of the HbRC or resides in the bulk micelles.

During the optimization of the purification protocol, we included 0.5 M NaCl at each step during membrane preparation, solubilization, and chromatography. This addition was designed to remove any peripheral membrane proteins, especially cytochrome *c*<sub>553</sub> and the PshB ferredoxins, which closely associate with the HbRC core. In the future, we will experiment with omitting the sodium chloride in the buffers in order to preserve the peripheral membrane proteins.

An important conclusion of this study is the lack of effect of the introduced tags beyond their intended function of facilitating purification via affinity chromatography. We did observe some smaller polypeptides in preparations of each tagged variant (especially in the IH-IH-HbRC, Fig. 4), indicating that the tagged PshA may be subject to slightly more proteolysis than WT PshA, or that proteolysis products maintaining the tags are pulled down during affinity chromatography. However, the lack of effect upon total photochemical activity indicates that the HbRCs purified by virtue of their attached tag did not contain a significant fraction of inactive complexes. Moreover, neither tag had an observable effect upon photosynthetic growth.

This indicates that the tags do not affect ferredoxin binding to the HbRC. Defects in either photochemistry or ferredoxin binding to the HbRC would have been apparent in the growth rate, with growth more resembling the parental  $\Delta pshA::cbp2p-aph3$  strain (Supplementary Information, Fig. S1).

Another conclusion of this study was that the final cell density, rather than the doubling time, correlated better with increasing HbRC content (Fig. 4 and Fig. S1). A working hypothesis is that *Hbt. modesticaldum* maintains a constant growth rate until a nutrient becomes limiting. In the dark, they generate ATP via substrate-level phosphorylation, oxidizing pyruvate to acetyl-CoA and CO<sub>2</sub>; the former is converted to acetyl-phosphate, which is used as a phosphate donor to ADP in the reaction catalyzed by acetate kinase (Tang et al. 2010). In the light, *Hbt. modesticaldum* can make ATP via light-driven cyclic electron flow and thus can divert some pyruvate for other uses, such as generating biomass. While the  $\Delta pshA::cbp2p-aph3$  mutant grows in the light as the WT does in the dark (Baker et al. 2019a), the rescued strains grow in the light to levels intermediate between  $\Delta pshA::cbp2p-aph3$  and WT, indicating a mixed metabolism utilizing both cyclic photophosphorylation and substrate-level phosphorylation. Cells likely stop growing when they run out of pyruvate, which is the sole reduced carbon source in PYE medium. Taking these lines of evidence together, the less that *Hbt. modesticaldum* uses pyruvate as an energy source (*i.e.*, the more it makes use of cyclic photophosphorylation), the longer the pyruvate will last, and *Hbt. modesticaldum* can thus grow for a longer time and accomplish more cell divisions.

The finding that HbRC accumulated poorly when the vector-borne copy of the *pshA* gene was driven by fragments of DNA found upstream of *pshA* in the chromosome (Fig. 3) seemingly contradicts recent transcriptomic data. These data showed that the *pshA* transcript level is one of the highest of any protein-coding sequence in the cell, as well as noticeably higher than any of the transcripts coding for BChl-synthesis genes in the same photosynthetic gene cluster. Thus, these data implied that transcription of *pshA* is driven by its own strong promoter (Sheehy et al. 2018). To address this contradiction, we hypothesize that the main photosynthetic gene cluster in *Hbt. modesticaldum* (with genes in the following order: *bchJ-G*, *pshA*, *bchM-E-L-N-B-I-D-H*, and *crtN*) may be expressed at a relatively low level using a single promoter at the 5' end of the operon, but the 5'- or 3'-untranslated region of the *pshA* transcript is somehow stabilized and provides protection from degradation, thus allowing for the accumulation of a high steady-state transcript level. This idea draws inspiration from what is observed in various operons of the eukaryotic chloroplast (for a review, see (Manavski et al. 2018)). Future work should be dedicated to

specifically addressing the expression patterns of genes in the photosynthetic gene cluster.

The inversely proportional relationship between *pshA* expression and BPheo *g* accumulation also warrants discussion: the  $\Delta pshA::cbp2p-aph3$  strain essentially accumulates only BPheo *g* when grown under illumination, and as *pshA* expression returns to lower-than-WT levels in the rescued strains, BChl *g* accumulation returns and the amount of BPheo *g* decreases. We hypothesize a simple model to explain this. In *Hbt. modesticaldum*, it would seem that the amount of pigment (including BChl *g/g'*, 8<sup>1</sup>-OH Chl *a*, and 4,4'-DANS) and PshA polypeptide produced is a set amount dictated primarily by the presence of light and amount of available reduced nitrogen. Thus, any PshA polypeptide produced incorporates these pigments, and, if not enough PshA polypeptides are available to incorporate all the produced pigment, the remaining pigment is degraded. Since BPheo *g* is not an intermediate in the biosynthesis pathway of BChl *g/g'* or 8<sup>1</sup>-OH Chl *a* (Sattley et al. 2008; Ortega-Ramos et al. 2018), its accumulation points to its role as an intermediate in the BChl breakdown pathway. It would appear that Mg<sup>2+</sup> removal is the first step in this process, making BPheo *g* the first breakdown intermediate of BChl *g*. Correspondingly, 8<sup>1</sup>-OH Pheo *a* would be the first breakdown intermediate of 8<sup>1</sup>-OH Chl *a*. These intermediates accumulate in the cell membranes before presumably being defarnesylated (removal of farnesyl tail) and further broken down to pheophorbides and beyond. In addition, the amount of 4,4'-DANS in the cells seems to be constant no matter how much HbRC is present. It is reasonable to assume that accumulation of this pigment in the cell membranes is not detrimental to the organism.

The rest of the pathway for (B)Chl degradation in *Hbt. modesticaldum* is unknown, and similar pathways are generally unstudied in prokaryotic phototrophs. A search of the *Hbt. modesticaldum* genome using BLAST revealed no homologs to chlorophyllase, pheophytinase, the STAY-GREEN (magnesium dechetalase) proteins, or any other known enzymes implicated in the pheophorbide *a* oxygenase/phyllobilin recycling pathway (Hörtensteiner and Kräutler 2011; Shimoda et al. 2016) from algae or higher plants. It is therefore likely that the heliobacteria possess a different system for degrading (B)Chl. Since chlorophyllase and pheophytinase are part of a broad and common enzyme class, the serine-type hydrolases, the heliobacteria may have acquired new hydrolases or adapted pre-existing hydrolases to perform these chemistries. However, the fact that (B)Pheos accumulate in the  $\Delta pshA::cbp2p-aph3$  strain suggests that the (B)Chl degradation pathway is slow and may not use specialized proteins. Also, the continued production and breakdown of (B)Chls in the  $\Delta pshA::cbp2p-aph3$  strain when grown in the light may hinder cell fitness due to the high biosynthetic cost of (B)

Chl (primarily nitrogen and ATP) without energetic return (through successful phototrophy). This can be tested in future studies through growth trials in various nitrogen-depleted or carbon-depleted conditions.

In conclusion, other than allowing for a better retention of bound menaquinone, both methods of affinity-tagging the PshA polypeptide otherwise produced HbRC with identical function to that of the untagged, wild-type version. This implies that site-directed mutants designed to probe the function of the electron transfer cofactors can be produced and purified without the tags confounding measurements on photochemistry or structure. Additionally, the unexpected success of the internally-tagged version gives hope that the loop region in between TMH6 and TMH7 can be exploited for more aggressive mutagenesis, including attachment of molecular handles to the acceptor side of the HbRC, insertion of long regions to produce chimeras, or truncation of parts of the preceding antenna domain. Overall, we now have a suitable level of genetic and biochemical control to study the HbRC at the same level of depth as other photochemical reaction centers.

**Acknowledgements** The authors gratefully acknowledge support from the Division of Chemical Sciences, Geosciences, and Biosciences, Office of Basic Energy Sciences of the U.S. Department of Energy through grant DE-SC0010575 awarded to K.E.R.

## References

- Azai C, Kim K, Kondo T et al (2011) A heterogeneous tag-attachment to the homodimeric type I photosynthetic reaction center core protein in the green sulfur bacterium *Chlorobaculum tepidum*. *Biochim Biophys Acta* 1807:803–812. <https://doi.org/10.1016/j.bbabi.2011.03.007>
- Baker P, Orf GS, Kevershan K et al (2019a) Using the endogenous CRISPR-Cas system of heliobacteria to delete the photochemical reaction center core subunit gene. *Appl Environ Microbiol*. <https://doi.org/10.1128/AEM.01644-19>
- Baker P, Orf GS, Khan Z et al (2019b) A molecular biology toolkit for the photosynthetic Firmicute, *Heliobacterium modesticaldum* Ice1. *Appl Environ Microbiol*. <https://doi.org/10.1128/AEM.01287-19>
- Blankenship RE (2014) *Molecular mechanisms of photosynthesis*, 2nd edn. Wiley, Southern Gate
- Bryant DA, Frigaard N-U (2006) Prokaryotic photosynthesis and phototrophy illuminated. *Trends Microbiol* 14:488–496. <https://doi.org/10.1016/j.tim.2006.09.001>
- Chevallet M, Luche S, Rabilloud T (2006) Silver staining of proteins in polyacrylamide gels. *Nat Protoc* 1:1852–1858. <https://doi.org/10.1038/nprot.2006.288>
- Fischer WW, Hemp J, Johnson JE (2016) Evolution of oxygenic photosynthesis. *Annu Rev Earth Planet Sci* 44:647–683. <https://doi.org/10.1146/annurev-earth-060313-054810>
- Garnier T, Cole S (1988) Complete nucleotide sequence and genetic organization of the bacteriocinogenic plasmid, pIP404, from *Clostridium perfringens*. *Plasmid* 150:134–150
- Gisriel C, Sarrou I, Ferlez B et al (2017) Structure of a symmetric photosynthetic reaction center-photosystem. *Science* 357:1021–1025. <https://doi.org/10.1126/science.aan5611>
- Goldsmith JO, Boxer SG (1996) Rapid isolation of bacterial photosynthetic reaction centers with an engineered poly-histidine tag. *Biochim Biophys Acta* 1276:171–175. [https://doi.org/10.1016/0005-2728\(96\)00091-6](https://doi.org/10.1016/0005-2728(96)00091-6)
- Gulis G, Narasimhulu KV, Fox LN, Redding KE (2008) Purification of His6-tagged Photosystem I from *Chlamydomonas reinhardtii*. *Photosynth Res* 96:51–60. <https://doi.org/10.1007/s11120-007-9283-9>
- Heap JT, Pennington OJ, Cartman ST, Minton NP (2009) A modular system for Clostridium shuttle plasmids. *J Microbiol Methods* 78:79–85. <https://doi.org/10.1016/j.jmimet.2009.05.004>
- Heinrickel M, Golbeck JH (2007) Heliobacterial photosynthesis. *Photosynth Res* 92:35–53. <https://doi.org/10.1007/s11120-007-9162-4>
- Heinrickel M, Shen G, Agalarov R, Golbeck JH (2005) Resolution and reconstitution of a bound Fe-S protein from the photosynthetic reaction center of *Heliobacterium modesticaldum*. *Biochemistry* 44:9950–9960. <https://doi.org/10.1021/bi050588s>
- Heinrickel M, Shen G, Golbeck JH (2007) Identification and characterization of PshB, the dicluster ferredoxin that harbors the terminal electron acceptors FA and FB in *Heliobacterium modesticaldum*. *Biochemistry* 46:2530–2536. <https://doi.org/10.1021/bi0622165>
- Hörtensteiner S, Kräutler B (2011) Chlorophyll breakdown in higher plants. *Biochim Biophys Acta* 1807:977–988. <https://doi.org/10.1016/j.bbabi.2010.12.007>
- Kashey TS, Luu DD, Cowgill JC et al (2018) Light-driven quinone reduction in heliobacterial membranes. *Photosynth Res*. <https://doi.org/10.1007/s11120-018-0496-x>
- Kimble LK, Mandelco L, Woese CR, Madigan MT (1995) *Heliobacterium modesticaldum*, sp. nov., a thermophilic heliobacterium of hot springs and volcanic soils. *Arch Microbiol* 163:259–267. <https://doi.org/10.1007/BF00393378>
- Kondo T, Itoh S, Matsuoka M et al (2015) Menaquinone as the secondary electron acceptor in the Type I homodimeric photosynthetic reaction center of *Heliobacterium modesticaldum*. *J Phys Chem B* 119:8480–8489. <https://doi.org/10.1021/acs.jpcc.5b03723>
- Li C, Wen A, Shen B et al (2011) FastCloning: a highly simplified, purification-free, sequence- and ligation-independent PCR cloning method. *BMC Biotechnol* 11:92. <https://doi.org/10.1186/1472-6750-11-92>
- Manavski N, Schmid L-M, Meurer J (2018) RNA-stabilization factors in chloroplasts of vascular plants. *Essays Biochem* 62:51–64. <https://doi.org/10.1042/EBC20170061>
- Miyamoto R, Iwaki M, Mino H et al (2006) ESR signal of the iron-sulfur center FX and its function in the homodimeric reaction center of *Heliobacterium modesticaldum*. *Biochemistry* 45:6306–6316. <https://doi.org/10.1021/bi0519710>
- Miyamoto R, Mino H, Kondo T et al (2008) An electron spin-polarized signal of the P800 + A1(Q)- state in the homodimeric reaction center core complex of *Heliobacterium modesticaldum*. *Biochemistry* 47:4386–4393. <https://doi.org/10.1021/bi701612v>
- Olson DG, Maloney M, Lanahan AA et al (2015) Identifying promoters for gene expression in *Clostridium thermocellum*. *Metab Eng Commun* 2:23–29. <https://doi.org/10.1016/j.meteno.2015.03.002>
- Orf GS, Gisriel C, Redding KE (2018) Evolution of photosynthetic reaction centers: insights from the structure of the heliobacterial reaction center. *Photosynth Res* 138:11–37. <https://doi.org/10.1007/s11120-018-0503-2>
- Ortega-Ramos M, Canniffe DP, Radle MI et al (2018) Engineered biosynthesis of bacteriochlorophyll gF in *Rhodobacter sphaeroides*. *Biochim Biophys Acta* 1859:501–509. <https://doi.org/10.1016/j.bbabi.2018.02.006>
- Redding KE, Sarrou I, Rappaport F et al (2014) Modulation of the fluorescence yield in heliobacterial cells by induction of charge

- recombination in the photosynthetic reaction center. *Photosynth Res* 120:221–235. <https://doi.org/10.1007/s11120-013-9957-4>
- Sarrou I, Khan Z, Cowgill JB et al (2012) Purification of the photosynthetic reaction center from *Heliobacterium modesticaldum*. *Photosynth Res* 111:291–302. <https://doi.org/10.1007/s11120-012-9726-9>
- Sattley WM, Swingley WD (2013) Properties and evolutionary implications of the heliobacterial genome. In: Beatty JT (ed) *Advances in botanical research*, vol 66: genome evolution of photosynthetic bacteria. Academic Press, Amsterdam, pp 67–97
- Sattley WM, Madigan MT, Swingley WD et al (2008) The genome of *Heliobacterium modesticaldum*, a phototrophic representative of the Firmicutes containing the simplest photosynthetic apparatus. *J Bacteriol* 190:4687–4696. <https://doi.org/10.1128/JB.00299-08>
- Schägger H (2006) Tricine-SDS-PAGE. *Nat Protoc* 1:16–22. <https://doi.org/10.1038/nprot.2006.4>
- Sheehy D, Lu Y-K, Osman F et al (2018) Genome-wide transcriptional response during the shift to N<sub>2</sub>-fixing conditions in *Heliobacterium modesticaldum*. *J Proteomics Bioinform* 11:143–160. <https://doi.org/10.4172/jpb.1000481>
- Shevchenko A, Tomas H, Havlis J et al (2006) In-gel digestion for mass spectrometric characterization of proteins and proteomes. *Nat Protoc* 1:2856–2860. <https://doi.org/10.1038/nprot.2006.468>
- Shimoda Y, Ito H, Tanaka A (2016) Arabidopsis STAY-GREEN, Mendel's green cotyledon gene, encodes magnesium-dechelataase. *Plant Cell* 28:2147–2160. <https://doi.org/10.1105/tpc.16.00428>
- Siefermann-Harms D (1988) High-performance liquid chromatography of chloroplast pigments. *J Chromatogr A* 448:411–416. [https://doi.org/10.1016/S0021-9673\(01\)84604-5](https://doi.org/10.1016/S0021-9673(01)84604-5)
- Sloan J, Warner TA, Scott PT et al (1992) Construction of a sequenced *Clostridium perfringens*-*Escherichia coli* shuttle plasmid. *Plasmid* 27:207–219. [https://doi.org/10.1016/0147-619X\(92\)90023-4](https://doi.org/10.1016/0147-619X(92)90023-4)
- Sugiura M, Inoue Y (1999) Highly purified thermo-stable oxygen-evolving photosystem II core complex from the thermophilic cyanobacterium *Synechococcus elongatus* having His-Tagged CP43. *Plant Cell Physiol* 40:1219–1231. <https://doi.org/10.1093/oxfordjournals.pcp.a029510>
- Tang K-H, Feng X, Zhuang WQ et al (2010) Carbon flow of heliobacteria is related more to clostridia than to the green sulfur bacteria. *J Biol Chem* 285:35104–35112. <https://doi.org/10.1074/jbc.M110.163303>
- Trost JT, Blankenship RE (1989) Isolation of a photoactive photosynthetic reaction center-core antenna complex from *Heliobacillus mobilis*. *Biochemistry* 28:9898–9904
- van de Meent EJ, Kleinherenbrink FAM, Amesz J (1990) Purification and properties of an antenna-reaction center complex from heliobacteria. *Biochim Biophys Acta* 1015:223–230. [https://doi.org/10.1016/0005-2728\(90\)90024-X](https://doi.org/10.1016/0005-2728(90)90024-X)
- van de Meent EJ, Kobayashi M, Erkelens C et al (1991) Identification of 81-hydroxychlorophyll a as a functional reaction center pigment in heliobacteria. *Biochim Biophys Acta* 1058:356–362. [https://doi.org/10.1016/S0005-2728\(05\)80131-8](https://doi.org/10.1016/S0005-2728(05)80131-8)
- van der Est A, Hager-Braun C, Leibl W et al (1998) Transient electron paramagnetic resonance spectroscopy on green-sulfur bacteria and heliobacteria at two microwave frequencies. *Biochim Biophys Acta* 1409:87–98. [https://doi.org/10.1016/S0005-2728\(98\)00152-2](https://doi.org/10.1016/S0005-2728(98)00152-2)

**Publisher's Note** Springer Nature remains neutral with regard to jurisdictional claims in published maps and institutional affiliations.